Assessment of flow aggressiveness at an ultrasonic horn cavitation erosion test device by PVDF pressure measurements and 3D flow simulations

[1]Simon A. Paepenmöller*; [1]Johannes Kuhlmann; [1]Martin Blume; [1]Romuald Skoda

[1] *Chair of Hydraulic Fluid Machinery, Ruhr-Universität Bochum, Universitätsstr. 150, 44801 Bochum, Germany*

Abstract

Transient cavitation induced loads are investigated in a flow region subject to severe cavitation erosion at an ultrasonic horn test facility operated in indirect mode, both experimentally and via CFD. A variation of gap width and sensor position is used to vary flow aggressiveness. The experimental technique utilizes piezoelectric sensors based on Polyvinylidene fluordide (PVDF). Sensors are employed at the stationary specimen in close proximity to the oscillating horn tip and wall load spectra are obtained. Complementary CFD studies emulate the experimental sensor. Flow aggressiveness decreases when the gap is widened and increases towards the stationary specimen center. Results from experiment and simulation show good quantitative agreement.

Keywords: cavitation erosion, wall load spectrum, PVDF sensor, CFD, barotropic equation of state

1. Introduction

Ultrasonic horns are widely used to characterize the resistance of materials to cavitation erosion. The test facility employs a horn oscillating in longitudinal mode at high frequency to cause generation and collapse of voids below the oscillating tip. We employ the indirect method, in which a stationary erosion sample is placed in close proximity to the tip. The gap width is an important parameter that influences erosion pattern, mass loss rate and incubation time of the erosion sample [1–3].

To gain better understanding of the erosion process, load measurements have been performed at ultrasonic horn facilities by different groups (see e.g., [4–8]). Wall load spectra are obtained by performing peak detection on the force signal, either as postprocessing or during runtime through hardware (i.e. a peak hold circuit with finite reset interval). Derived histograms are typically presented in cumulative form, with the occurrence rate normalized to measurement time and sensitive area of the sensor. Detected events show exponential distribution. This behavior is shared with other cavitation test facilities (see e.g., [9, 10]).

Within the present study, a variation of gap width and sensor position is used to adjust flow aggressiveness. Wall load spectra are determined from the experiment as well as from numerical simulation: the experiment utilizes piezoelectric PVDF-foil based sensors, which are reproduced within the simulation to reflect sensor position, size and spatial integrating behavior. Peak detection and derivation of load collectives is performed on both, signals from experiment and simulation with identical method and the resulting statistics are compared. The numerical approach is especially attractive, since the experiment's physical limit of spatial resolution (i.e. possible sensor miniaturization) is multiple orders of magnitude larger than the spatial limit of simulation (i.e. grid resolution). While high temporal resolution can be achieved in both, experiment and simulation, the latter is solely bounded by computational cost.

Aim of the present study is to evaluate CFD as a complimentary tool for flow aggressiveness assessment. For this purpose, experimental results are carefully examined in terms of reliability and repeatability. Quality of the simulation is assured through a grid refinement study and evaluation of temporal convergence of the obtained load collectives.

2. Experimental configuration

The test facility consists of a commercially available ultrasonic horn from Hielscher Ultrasonics (UIP2000hd) operated at 19.8 kHz driving frequency and 40.9µm amplitude (peak-to-peak). The horn tip is immersed in distilled water at equilibrium air saturation, kept at 20°C by an actively controlled indirect cooling circuit, as shown in Fig. 1. Gap width between horn tip and the sensor equipped stationary specimen is adjusted with a 10µm precision leveling device.

*Corresponding Author, Simon A. Paepenmöller: simon.paepenmoeller@rub.de

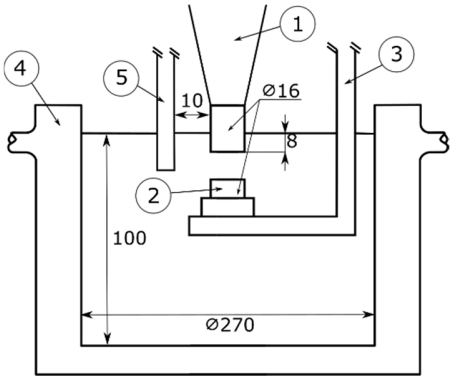

1. Ultrasonic horn
2. Stationary specimen
3. Leveling device
4. Cooling circuit
5. Temperature sensor

Fig. 1 Test facility with dimensions in mm.

2.1. Sensor design, calibration and signal processing

To enable temporal resolution of cavitation events, the sensors utilized follow a minimum thickness doctrine without attenuating backing layer. This design leads to maximized resonance frequency and bandwidth of the instrument. Preceding stages of instrument development have been published [11, 12] and the final design is depicted in Fig. 2. Upper and lower pole connect to a fully differential charge amplifier.

A piezoelectric PVDF foil element of 5mm diameter and 30µm thickness is laminated between an UV-cured resin as top layer, and a bottom layer made from Polyethylene terephthalate (PET). Electrodes are printed in a screen printing technique and the top layer erosion resistance is improved through a single layer of Polyimide (Kapton) adhesive tape. The overall package height is 295±25µm.

Fig. 2 Sensor with electrodes on the left and sensitive area on the right.

The sensor outlines are milled into a stationary specimen and the foils are mounted flush with cyanoacrylate glue. The two investigated radial positions are shown in Fig. 3, where the sensitive area is depicted in dark grey.

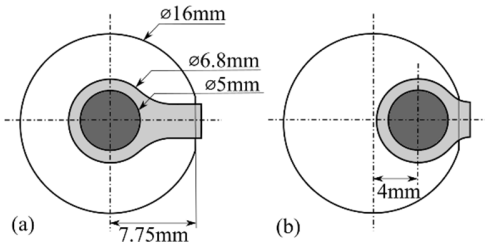

Fig. 3 Top view on stationary specimen with centric (a) and excentric (b) sensor mounting positions.

Calibration is performed with the ball drop technique, where a steel ball is dropped unto the surface from a predefined height and the rebound is measured through long exposure imaging. Contact time and amplitude are utilized to calculate the time averaged force during contact from momentum and energy conservation considerations. The calibration constant of the sensor is determined from 10 repetitions at approximately 40 N loading and 26 µs contact time. Repeatability of the mean calibration constant is about ±5%.

The voltage signal is digitized with a 12 bit deep memory high-speed oscilloscope at 15.63 MHz sampling rate for a continuous interval of at least 7 s. As the sensor surface is not loaded uniformly, we are limited to the quantification of integral force across the sensor surface. Peak detection is performed with an algorithm utilizing a minimum amplitude threshold of 10 N, a peak prominence value of 10 N and a minimum peak distance of 0.26µs. It is performed on the raw signals without smoothing or band pass filter operations. Reasonable lower bounds for threshold and

*Corresponding Author, Simon A. Paepenmöller: simon.paepenmoeller@rub.de

prominence depend on the signal to noise ratio, while introducing a minimum peak distance has shown to improve detection quality and increase robustness. Negligible influence of the parameters has been assured through variation.

Sensors are subject to severe erosion and subsequent destruction or alteration of characteristics. We ensured reliability of the results by limiting usage time of each sensor to 8 s and applying them in a one-way manner. We performed reproduction at every operating point with a new sensor and ensured unaltered characteristics through recalibration after each run. We further ensured that the final load collectives are not subject to systematic temporal effects by splitting the force signal into 0.5 s chunks and deriving statistics from the pieces: if the collectives obtained in this manner show only slight variation around a stable mean, we assume that no degenerative effects are present.

3. Numerical method and numerical sensor

For the numerical part we perform explicit 3rd order Runge-Kutta time integration of the Euler equations for an inviscious fluid, coupled with an isentropic barotropic equation of state, in finite volume discretization with flux-corrected, conservative mesh deformation. A homogenous mixture of liquid and vapor within each cell is assumed. The method has previously been implemented into our in-house code 'Hydrub' and applied to study erosion sensitive wall zones and erosion mechanisms at ultrasonic horns [13]. By counting events exceeding threshold values for pressure and void collapse rate, erosion indicators and a map of dimensionless erosion probability are obtained. Details on the numerical scheme and the assessment of erosion sensitive wall zones by erosion probability can be found in Mottyll and Skoda [13]. Results within the present publication are generated with our in-house OpenFOAM implementation 'HydrubFOAM' [14]. For density, the Minmod scheme [15] is employed, while for velocity the GammaV scheme [16] is utilized to provide 2nd order accuracy in space.

The numeric domain mimics the experimental geometry depicted in Fig. 1. Simulation time step depends on the acoustic CFL number and therefore depends on the smallest cell within the domain: it is typically about 13 ns for basic mesh settings and 6.4 ns for refined meshes.

Cell faces of the stationary specimen top wall (i.e. numerical domain boundary faces), are grouped to a numeric sensor in accordance with the experimental sensor's position and size. Through integration of numerical cell face center pressure across the numerical sensor, a force signal is obtained in analogy to the experiment.

For the excentric position, 5 numerical sensors are deployed along the circumference and their signals are concatenated in order to provide virtually extended evaluation time. The algorithm and parameters used to derive the load collectives are identical for both numerical and experimental input data.

3.1. Grid quality and grid independency

Utilized grids are generated block structured with combined H- and O-grid topology. The grid within the gap and its immediate surrounding is optimized for minimal distortion and volume change. This is a necessary prerequisite for the erosion indicator methodology (as described in [13]). Cell volumes within the entire gap differ by ±12 % from average. Grids for all gap widths investigated share a constant cell height of 50 µm (basic mesh) respectively 25 µm (refined mesh) throughout the cavitation zone. To reduce computational effort, hanging nodes and volume expansion are employed outside the cavitation zone, i.e. the beaker geometry. The total number of cells is approximately 110k for coarse and 430k for refined grids.

Previous employment of a closely related numerical technique at hydrodynamic cavitation test facility has revealed strong mesh dependency of the numerical sensor results [17]. Our grid study proves only minor influence of the grid resolution, as depicted in Fig. 4, where collapse force rates are shown, i.e. the normalized cumulated rate of peaks exceeding a certain force. Loading of the stationary specimen is dominated by subharmonic collapse, i.e. the collapse of large vapor structures which form over a multiple of the horn driving period [13]. The weak grid dependence of numerical sensor signals presented here is attributed to the large sensor size: while numerical pressure in a single cell strongly depends on grid size, cell-face area weighted integration across a large number of cells to obtain a sensor force diminishes grid dependency. Preliminary simulations have shown, that a much smaller numerical sensor exhibits significant grid dependence, also at ultrasonic horn test cases.

All subsequently presented results have been obtained on the coarser grid.

*Corresponding Author, Simon A. Paepenmöller: simon.paepenmoeller@rub.de

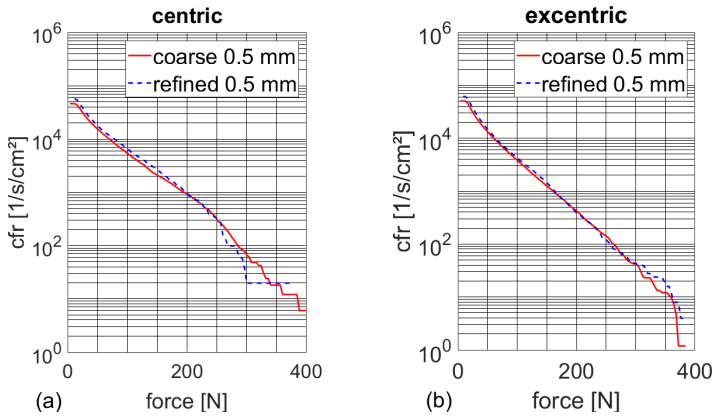

Fig. 4 Load collectives from centric (a) and excentric (b) positioned sensors for coarse and refined meshes at simulation time 0.75 s (coarse) and 0.26 s (refined). The excentric signal measurement time is extended through concatenation of 5 virtual probes.

3.2. Temporal convergence

When deriving load collectives from successively prolonged experimental data, results become indistinguishable after approximately 3 s. The computational effort of the simulation does not allow for such a period to be evaluated, but sufficient convergence in the numerical study is achieved faster, typically after approximately 0.5 s. All subsequently presented results are ensured to be temporally converged.

4. Results

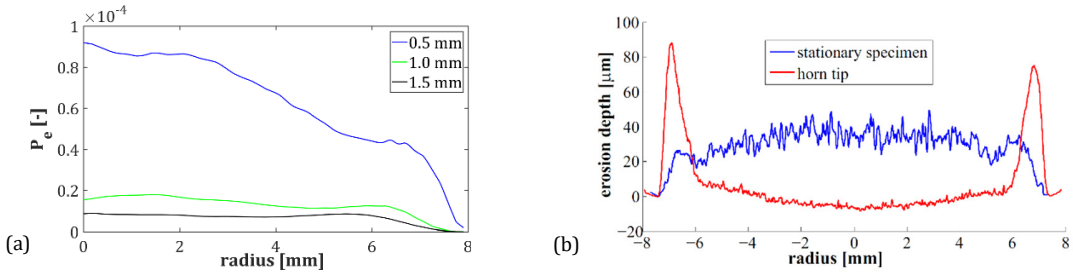

Fig. 5 (a): Radial erosion probability (P_E) distribution on the stationary specimen from simulation for varying gap widths and (b) erosion depths as measured for 0.5mm gap width (Part b reprinted from [13]).

The erosion indicator methodology predicts increasing erosion probability towards the center of the stationary specimen for 0.5 mm gap width, as shown in Fig. 5 (a): this is in good agreement with practical experience as well as topographic measurements, as reprinted in Fig. 5 (b) from [13], where the erosion depth for the stationary specimen and horn tip is shown.

*Corresponding Author, Simon A. Paepenmöller: simon.paepenmoeller@rub.de

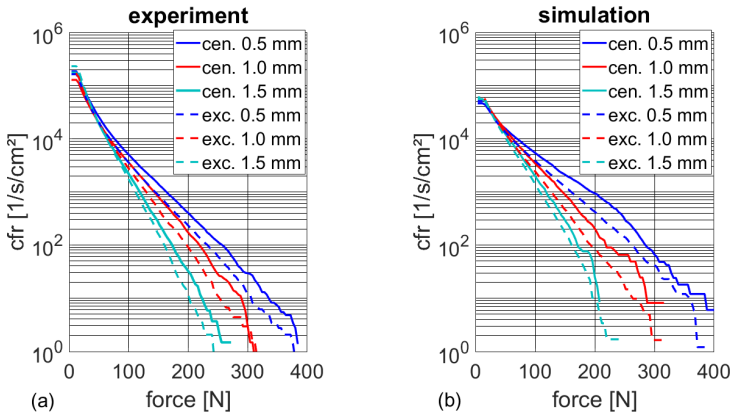

Fig. 6 Load collectives in dependence of gap width and radial position from experiment (a) and simulation (b).

Widening of the gap leads to reduced flow aggressiveness, manifesting itself in a decrease of erosion probability (see Fig. 5 a) and a decrease of the slope of the load collectives, as presented in Fig. 6. This result is confirmed by erosion tests performed at our laboratory, which show prolonged incubation time and reduced steady state mass loss rate for increased gap width (exemplarily data given for 1.4404 steel in Table 1). The flow aggressiveness measured in excentric position is decreased in comparison to the centric position, as seen in Fig. 6 (a). Simulation results reproduce this behavior, depicted in Fig. 6 (b).

Table 1 Erosion testing results of polished 1.4404 specimen in distilled water @20°C, 41µm amplitude and 19.8kHz frequency

Gap width [mm]	**0.5**	**1.0**	**1.5**
Incubation time [s]	8600	8800	12600
Steady state erosion rate [µg/min]	48	32	18

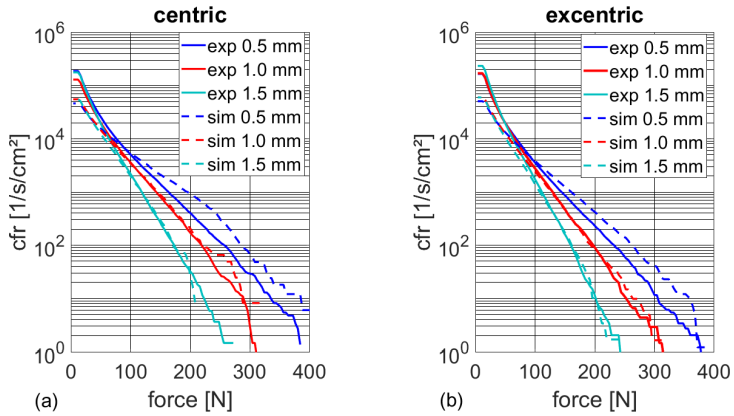

Fig. 7 Load collectives from experiment and simulation in dependence of gap width for centric (a) and excentric (b) position.

Quantitative comparison of the load collectives from experiment and simulation is given in Fig. 7. The total number of events (i.e. the vertical axis intercept) in the simulation is lower than in the experiment. For gap widths of 1.0 mm and 1.5 mm the characteristic slope is reproduced very well. For 0.5 mm there is an offset of the collective. We assume that the poorer match at 0.5 mm is due to neglect of non-condensable gas in the simulation. This assumption is further supported by preliminary measurements, which reveal a stagnation of flow aggressiveness for gaps below 0.5 mm, while the simulation results indicate increasing flow aggressiveness. Of course this hypothesis is yet speculative and demands further investigation.

*Corresponding Author, Simon A. Paepenmöller: simon.paepenmoeller@rub.de

5. Conclusion

The numerical method has proven capability to correctly account for the influence of gap width and radial position. Although the vertical axis intercept (i.e. the total number of events) differs between experimental and numerical study, the operating conditions can be correctly assessed by the load collective slope. Extrapolation of the linear part of the simulation collectives can be used to compensate the intercept mismatch. Forces predicted from the simulation are in good quantitative agreement with experimental values and we therefore conclude CFD to be established as a complimentary method to impact load measurement.

Further work will concern smaller gap widths, which might require extending the numerical model to incorporate effects such as the presence of non-condensable gas. Future investigation should establish a link between assessed flow aggressiveness and material response, i.e. validation of an erosion model based on localized impact load distributions.

6. References

[1] Endo, K., Okada, T., Nakashima, M. (1967). *A Study of Erosion Between Two Parallel Surfaces Oscillating at Close Proximity in Liquids.* J. Lub. Tech.; 89: 229.

[2] Kikuchi, K., Hammitt, F. G. (1985). *Effect of separation distance on cavitation erosion of vibratory and stationary specimens in a vibratory facility.* Wear; 102: 211–25.

[3] Matsumara, M., Okumoto, S., Saga, Y. (1982). *Mechanism of Damage in the Vibratory Test with Stationary Specimen.* Bulletin of JSME; 25: 898–905.

[4] Okada, T., Iwai, Y., Awazu, K. (1989). *A study of cavitation bubble collapse pressures and erosion part 1:* A method for measurement of collapse pressures. Wear; 133: 219–32.

[5] Hattori, S., Mori, H., Okada, T. (1998). *Quantitative Evaluation of Cavitation Erosion.* J. Fluids Eng.; 120: 179.

[6] Arndt, R. E. A., Paul, S., Ellis, C. R. (1997). *Application of Piezoelectric Film in Cavitation Research.* Journal of Hydraulic Engineering; 123: 539–48.

[7] Lee, M. K., Hong, S. M., Kim, G. H., Kim, K. H., Rhee, C. K., Kim, W. W. (2006). *Numerical correlation of the cavitation bubble collapse load and frequency with the pitting damage of flame quenched Cu–9Al–4.5Ni–4.5Fe alloy.* Materials Science and Engineering: A; 425: 15–21.

[8] Singh, S., Choi, J.-K., Chahine, G. L. (2013). *Characterization of Cavitation Fields From Measured Pressure Signals of Cavitating Jets and Ultrasonic Horns.* J. Fluids Eng.; 135: 91302.

[9] Franc, J.-P., Riondet, M., Karimi, A., Chahine, G. L. (2011). *Impact Load Measurements in an Erosive Cavitating Flow.* J. Fluids Eng.; 133: 121301.

[10] De, M. K., Hammitt, F. G. (1982). *New Method for Monitoring and Correlating Cavitation Noise to Erosion Capability.* J. Fluids Eng.; 104: 434.

[11] Lang, S., Dimitrov, M., Pelz, P. F. (2012). *Spatial and Temporal High Resolution Measurement of Bubble Impacts. In:* Ohl C-D, editor. CAV 2012: Proceedings of the 8th International Symposium on Cavitation, 13 - 16 August 2012, Singapore. Singapore: Research Publishing Services.

[12] Dimitrov, M. (2015). *Räumlich auflösende, dynamische Druckmesssysteme mit piezoelektrischen Foliensensoren (In German)*. Aachen: Shaker.

[13] Mottyll, S., Skoda, R. (2016). *Numerical 3D flow simulation of ultrasonic horns with attached cavitation structures and assessment of flow aggressiveness and cavitation erosion sensitive wall zones.* Ultrason Sonochem; 31: 570–89.

[14] Deimel, C., Skoda, R. (2014). *Implementation of an explicit density-based solver for the simulation of cavitating flows in OpenFOAM*. 9th OpenFOAM Workshop Zagreb.

[15] Harten, A. (1983). *High resolution schemes for hyperbolic conservation laws.* Journal of Computational Physics; 49: 357–93.

[16] Jasak, H., Weller, H. G., Gosman, A. D. (1999). *High resolution NVD differencing scheme for arbitrarily unstructured meshes.* Int. J. Numer. Meth. Fluids; 31: 431–49.

[17] Mihatsch, M. S., Schmidt, S. J., Adams, N. A. (2015). *Cavitation erosion prediction based on analysis of flow dynamics and impact load spectra.* Physics of Fluids; 27: 103302.

*Corresponding Author, Simon A. Paepenmöller: simon.paepenmoeller@rub.de